Unexplained Excess of Electron-Like Events From a 1-GeV Neutrino Beam

A. A. Aguilar-Arevalo[5], C. E. Anderson[18], A. O. Bazarko[15], S. J. Brice[7], B. C. Brown[7], L. Bugel[5], J. Cao[14], L. Coney[5], J. M. Conrad[5,13], D. C. Cox[10], A. Curioni[18], Z. Djurcic[5], D. A. Finley[7], B. T. Fleming[18], R. Ford[7], F. G. Garcia[7], G. T. Garvey[11], C. Green[7,11], J. A. Green[10,11], T. L. Hart[4], E. Hawker[3,11], R. Imlay[12], R. A. Johnson[3], G. Karagiorgi[5,13], P. Kasper[7], T. Katori[10], T. Kobilarcik[7], I. Kourbanis[7], S. Koutsoliotas[2], E. M. Laird[15], S. K. Linden[18],J. M. Link[17], Y. Liu[14], Y. Liu[1], W. C. Louis[11], K. B. M. Mahn[5], W. Marsh[7], G. McGregor[11], W. Metcalf[12], P. D. Meyers[15], F. Mills[7], G. B. Mills[11], J. Monroe[5,13], C. D. Moore[7], R. H. Nelson[4], V. T. Nguyen[5,13], P. Nienaber[16], J. A. Nowak[12], S. Ouedraogo[12], R. B. Patterson[15], D. Perevalov[1], C. C. Polly[9,10], E. Prebys[7], J. L. Raaf[3], H. Ray[8,11], B. P. Roe[14], A. D. Russell[7], V. Sandberg[11], R. Schirato[11], D. Schmitz[5], M. H. Shaevitz[5], F. C. Shoemaker[15], D. Smith[6], M. Soderberg[18], M. Sorel[5*], P. Spentzouris[7], I. Stancu[1], R. J. Stefanski[7], M. Sung[12], H. A. Tanaka[15], R. Tayloe[10], M. Tzanov[4], R. Van de Water[11], M. O. Wascko[12†], D. H. White[11], M. J. Wilking[4], H. J. Yang[14], G. P. Zeller[5,11], E. D. Zimmerman[4]

(The MiniBooNE Collaboration)

[1] *University of Alabama; Tuscaloosa, AL 35487*

[2] *Bucknell University; Lewisburg, PA 17837*

[3] *University of Cincinnati; Cincinnati, OH 45221*

[4] *University of Colorado; Boulder, CO 80309*

[5] *Columbia University; New York, NY 10027*

[6] *Embry Riddle Aeronautical University; Prescott, AZ 86301*

[7] *Fermi National Accelerator Laboratory; Batavia, IL 60510*

[8] *University of Florida; Gainesville, FL 32611*

[9] *University of Illinois; Urbana, IL 61801*

[10] *Indiana University; Bloomington, IN 47405*

* Present Address: IFIC, Universidad de Valencia and CSIC, Valencia 46071, Spain

† Present address: Imperial College London, London, UK

[11] *Los Alamos National Laboratory; Los Alamos, NM 87545*

[12] *Louisiana State University; Baton Rouge, LA 70803*

[13] *Massachusetts Institute of Technology; Cambridge, MA 02139*

[14] *University of Michigan; Ann Arbor, MI 48109*

[15] *Princeton University; Princeton, NJ 08544*

[16] *Saint Mary's University of Minnesota; Winona, MN 55987*

[17] *Virginia Polytechnic Institute & State University; Blacksburg, VA 24061*

[18] *Yale University; New Haven, CT 06520*

(Dated: December 23, 2008)

Abstract

The MiniBooNE Collaboration observes unexplained electron-like events in the reconstructed neutrino energy range from 200 to 475 MeV. With 6.46×10^{20} protons on target, 544 electron-like events are observed in this energy range, compared to an expectation of 415.2 ± 43.4 events, corresponding to an excess of $128.8 \pm 20.4 \pm 38.3$ events. The shape of the excess in several kinematic variables is consistent with being due to either ν_e and $\bar{\nu}_e$ charged-current scattering or to ν_μ neutral-current scattering with a photon in the final state. No significant excess of events is observed in the reconstructed neutrino energy range from 475 to 1250 MeV, where 408 events are observed compared to an expectation of 385.9 ± 35.7 events.

In a previous Letter [1], the MiniBooNE collaboration reported initial results on a search for $\nu_\mu \rightarrow \nu_e$ oscillations. The search was motivated by the LSND observation [2] of an excess of $\bar{\nu}_e$ events in a $\bar{\nu}_\mu$ beam that implied larger values of Δm^2 than any of the currently confirmed oscillation measurements. The MiniBooNE result showed no evidence of an excess of electron-like events for neutrino energies above 475 MeV. However, a sizeable excess of electron-like events was observed from 300-475 MeV. This Letter reports on a more detailed investigation of the low-energy electron-like events [3]. Published explanations for the low-energy excess range from anomaly mediated neutrino-photon coupling [4] to neutrino oscillations involving sterile neutrinos [5, 6, 7, 8, 9] to Lorentz violation [10]. In the course of this investigation, many improvements have been made to the data analysis, and the data sample has increased from 5.58×10^{20} protons on target (POT) to 6.46×10^{20} POT. The excess of electron-like events persists after these improvements and has been studied as a function of several kinematic variables.

MiniBooNE uses the Fermilab Booster neutrino beam, which is generated from 8-GeV kinetic energy protons incident on a beryllium production target. Neutrinos are produced in a 50 m long decay pipe by the in-flight decay of pions and kaons and a small fraction of the subsequent muons. The center of the MiniBooNE detector is 541 m from the production target [11]. The neutrino target and detector medium is mineral oil in which relativistic particles create both Cherenkov and scintillation light. The different properties of these sources of light readily allow particle identification; however, the detector cannot distinguish between electrons and photons.

The Booster neutrino beam flux at the detector is modeled using a GEANT4-based simulation [12] of the beamline. Pion and kaon production in the target is parametrized [13] by a global fit to proton-beryllium particle production data [14, 15]. The ν_μ energy spectrum peaks at ~ 600 MeV, has a mean energy of ~ 800 MeV, and extends to ~ 3000 MeV [16].

The specific changes to the analysis of the low-energy events since the initial paper [1] are listed below and will be discussed in some detail in the following text.

- New data on π^0 production has been incorporated along with an improved determination of Δ radiative decays as constrained by observed neutral-current (NC) π^0 events.

- Photonuclear interactions in the detector medium are now included in the MiniBooNE GEANT3 simulation along with the final states they produce.
- An improved estimate of the background from external events has been made and a new cut is introduced that significantly reduces this contribution.
- Improvements to the determination of systematic errors have been made.
- A lower neutrino energy threshold of 200 MeV is used.

The v3 NUANCE [17] event generator is used to simulate neutrino interactions in mineral oil. The constraint on NC π^0 production from MiniBooNE data was expanded to finer momentum bins [18]. Also, a direct measurement of low energy NC coherent π^0 production [18] was implemented to improve the modeling of π^0 events in the most forward direction. In addition, there is a more accurate treatment of the ratio of γ to π^0 decay of Δ in nuclei. To avoid uncertainties in neutrino flux and NC cross sections, the number of Δ radiative decays is determined from the number of measured NC π^0 events.

Final state particles from the initial neutrino interaction [17], their decays, and possible strong and electromagnetic re-interactions in the detector medium are modeled using a GEANT3-based [19] simulation, with strong interactions simulated using GCALOR [20]. Since the previous Letter [1], a number of processes, missing from the strong interaction model, have been added that could create electron-like backgrounds: photonuclear interactions on carbon, radiative π^- capture, radiative decay of Δ resonances produced in pion-carbon interactions, and $\pi^{\pm}$-C (strong) elastic scattering. Radiative capture and $\Delta \to N\gamma$ decay produce single photons that MiniBooNE cannot distinguish from electrons. Photonuclear interactions can cause a photon from a π^0 to be missed, leaving a single photon. Elastic scattering of charged pions can cause Cherenkov rings to appear more electron-like. Of these, only photonuclear interactions contribute significantly to the electron-like background with apparent neutrino energy > 200 MeV. The well-measured photonuclear cross section on carbon is used to simulate final states from excitation of the giant dipole resonance and Δ production above and below the pion threshold. The addition of photonuclear absorption increases the estimated background from NC π^0 scattering by $\sim 30\%$ in the energy range $200 < E_\nu^{QE} < 475$ MeV. E_ν^{QE} is the reconstructed incident neutrino energy and is determined from the reconstructed lepton energy and angle with respect to the known neutrino

direction, assuming charged-current quasi-elastic (CCQE) scattering.

One of the larger $\nu_{\rm e}$ backgrounds at low energy results from neutrino interactions in the tank wall and concrete vault and dirt surrounding the detector. These events originating outside the detector are uniquely characterized by low visible energy (E_{vis}), large radius, and a direction that points into the detector; therefore, their contribution can be measured from MiniBooNE data. An improved estimate of this background using reconstructed event position and direction information reduces the normalization of such backgrounds by 30%. In addition, a new selection criterion based on energy and topology rejects 83% of these events, while discarding only 21% of signal events in the $200 < E_\nu^{QE} < 475$ MeV energy range.

Numerous improvements have been incorporated in the systematic error determination associated with the neutrino flux, detector, and neutrino cross section modeling. In estimating neutrino flux uncertainties, the propagation of π^+ production errors has been upgraded to remove unnecessary model dependence. This results in a decrease in the overall π^+ production uncertainty from $\sim 16\%$ to $\sim 7\%$ [16], which better reflects the uncertainties in the underlying HARP measurement of π^+ production on Be [14]. In the detector simulation, a comprehensive set of final state variations has been evaluated to conservatively encompass the uncertainty in the aforementioned list of added hadronic processes. These uncertainties contribute an additional 1% uncertainty in the low energy MiniBooNE oscillation analysis. In the neutrino cross section model, the estimation of the Δ radiative decays uncertainty has increased from 9% to 12%. Also, measurements of the rates of coherently and resonantly produced π^0 events [18] has enabled some reduction in these errors.

The reconstruction and selection of electron-like events is almost identical to the initial analysis [1]. Events are reconstructed under four hypotheses: a single electron-like Cherenkov ring, a single muon-like ring, two photon-like rings with unconstrained kinematics, and two photon-like rings with an invariant mass $M_{\gamma\gamma} = m_{\pi^0}$. To select ν_e-candidate events, an initial selection is first applied: > 200 tank hits, < 6 veto hits, one and only one event within the 19.2μs trigger window, reconstructed time within the neutrino beam spill, and $E_{vis} > 140$ MeV. The electron-hypothesis event vertex and muon-hypothesis track endpoint are then required to occur at radii < 500 cm and < 488 cm, respectively, to ensure good event reconstruction and efficiency for possible muon decay electrons. Particle identification cuts are then applied to reject muon and π^0 events. These are E_{vis}-dependent cuts

on $\log(L_e/L_\mu)$, $\log(L_e/L_{\pi^0})$, and $M_{\gamma\gamma}$, where L_e, L_μ, and L_{π^0} are the likelihoods for each event maximized under the electron 1-ring, muon 1-ring, and fixed-mass 2-ring fits, and $M_{\gamma\gamma}$ is from the unconstrained two-ring fit. These cuts were set prior to unblinding the original analysis and were not changed. In addition, a new cut is imposed to reject events produced outside the detector, as discussed earlier.

Four different analyses are performed on the data.

- Original Analysis: original analysis [1] with the original data set of 5.58×10^{20} POT.
- Revised Analysis: the Original Analysis with the updated background and uncertainty estimates described in this paper.
- Extended Analysis: the Revised Analysis but with the extended data set of 6.46×10^{20} POT.
- Final Analysis: the Extended Analysis but including the new external event cut.

Table I shows the expected number of events with E_ν^{QE} between $200-300$ MeV, $300-475$ MeV, and $475-1250$ MeV after the complete event selection of the Final Analysis. The background estimates include antineutrino events, representing $< 2\%$ of the total. The total expected backgrounds for the three energy regions are 186.8 ± 26.0 events, 228.3 ± 24.5 events, and 385.9 ± 35.7 events, respectively.

A total of 1069 events pass the complete event selection of the Final Analysis with $E_\nu^{QE} > 200$ MeV. The numbers of data, background, and excess events for different E_ν^{QE} ranges are shown in Table II, together with the significance of the excesses for the four analyses. The uncertainties include both statistical and systematic errors. While there is no significant event excess for $E_\nu^{QE} > 475$ MeV, a sizeable excess is observed for $E_\nu^{QE} < 475$ MeV. For the Final Analysis, an excess of $128.8 \pm 20.4 \pm 38.3$ events (3.0σ) is observed for $200 < E_\nu^{QE} < 475$ MeV.

Figure 1 shows the E_ν^{QE} distribution for data (points with statistical errors) and backgrounds (histogram with systematic errors) for the Final Analysis, and Fig. 2 shows the event excess as a function of E_ν^{QE}. Also shown in the figure, for comparison, are expectations from the best oscillation fit and from neutrino oscillation parameters in the LSND allowed region [2], which are ruled out at 95% CL if the data are fit with $E_\nu^{QE} > 475$ MeV [1]. The error bars include both statistical and systematic errors. The best ocillation fit for $E_\nu^{QE} > 200$

TABLE I: *The expected number of events in the* $200 < E_\nu^{QE} < 300$ *MeV,* $300 < E_\nu^{QE} < 475$ *MeV, and* $475 < E_\nu^{QE} < 1250$ *MeV energy ranges from all of the backgrounds after the complete event selection of the Final Analysis.*

Process	$200-300$	$300-475$	$475-1250$
ν_μ CCQE	9.0	17.4	11.7
$\nu_\mu e \to \nu_\mu e$	6.1	4.3	6.4
NC π^0	103.5	77.8	71.2
NC $\Delta \to N\gamma$	19.5	47.5	19.4
External Events	11.5	12.3	11.5
Other Events	18.4	7.3	16.8
ν_e from μ Decay	13.6	44.5	153.5
ν_e from K^+ Decay	3.6	13.8	81.9
ν_e from K_L^0 Decay	1.6	3.4	13.5
Total Background	186.8 ± 26.0	228.3 ± 24.5	385.9 ± 35.7

MeV corresponds to $\Delta m^2 = 3.14$ eV^2 and $\sin^2 2\theta = 0.0017$ and has a $\chi^2/DF = 18.3/17$. The null fit has a $\chi^2/DF = 22.0/19$. For $E_\nu^{QE} > 475$ MeV, the best fit is consistent with the initial result of no oscillations [1]. As shown in Fig. 3 for $E_\nu^{QE} > 200$ MeV, the event excess occurs for $E_{vis} < 400$ MeV.

Figs. 4 and 5 show the event excess as functions of reconstructed Q^2 and $\cos(\theta)$ for $300 < E_\nu^{QE} < 475$ MeV, the energy region with the most significant excess. Q^2 is determined from the energy and angle of the outgoing lepton, assuming CCQE scattering, and θ is the angle between the incident neutrino and outgoing lepton. Also shown in the figures are the expected shapes from the NC π^0 and $\Delta \to N\gamma$ reactions, which are representative of photon events produced by NC scattering, and from $\nu_e C \to e^- X$ and $\bar{\nu}_e C \to e^+ X$ CC scattering. The different reactions all assume the same ν_μ energy spectrum. As shown in Table III, the χ^2 values from comparisons of the event excess to the expected shapes are acceptable for all of the processes. Also shown in the table is the factor increase necessary for each process to explain the low-energy excess. In each case, the estimated background would have to more than double (increase by $> 5\sigma$) to explain the excess.

In summary, MiniBooNE observes an unexplained excess of $128.8 \pm 20.4 \pm 38.3$ electron-

TABLE II: *The number of data, background, and excess events for different E_ν^{QE} ranges, together with the significance of the excesses. The different analyses are described in the text.*

Event Sample	Original Analysis [1]	Revised Analysis	Extended Analysis	**Final Analysis**
$200-300$ MeV				
Data	375	368	427	232
Background	283 ± 37	332.4 ± 38.9	386.0 ± 44.3	186.8 ± 26.0
Excess (Significance)	92 ± 37 (2.5σ)	35.6 ± 38.9 (0.9σ)	41.0 ± 44.3 (0.9σ)	45.2 ± 26.0 (1.7σ)
$300-475$ MeV				
Data	369	364	428	312
Background	273 ± 26	282.9 ± 28.3	330.0 ± 31.8	228.3 ± 24.5
Excess (Significance)	96 ± 26 (3.7σ)	81.1 ± 28.3 (2.9σ)	98.0 ± 31.8 (3.1σ)	83.7 ± 24.5 (3.4σ)
$200-475$ MeV				
Data	744	732	855	544
Background	556 ± 54	615.3 ± 58.0	716.1 ± 66.2	415.2 ± 43.4
Excess (Significance)	188 ± 54 (3.5σ)	116.7 ± 58.0 (2.0σ)	138.9 ± 66.2 (2.1σ)	128.8 ± 43.4 (3.0σ)
$475-1250$ MeV				
Data	380	369	431	408
Background	358 ± 40	356.0 ± 33.3	412.7 ± 37.6	385.9 ± 35.7
Excess (Significance)	22 ± 40 (0.6σ)	13.0 ± 33.3 (0.4σ)	18.3 ± 37.6 (0.5σ)	22.1 ± 35.7 (0.6σ)

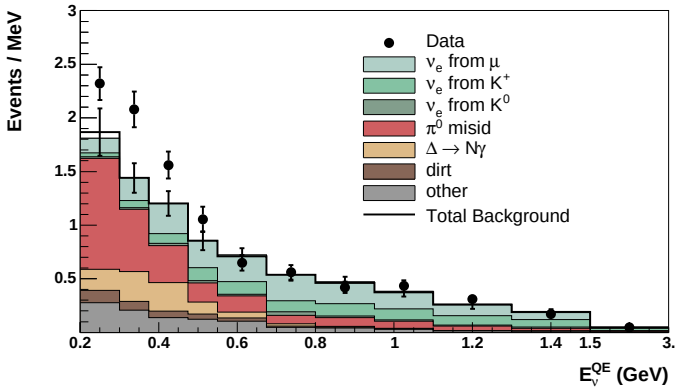

FIG. 1: The E_ν^{QE} distribution for data (points with statistical errors) and backgrounds (histogram with systematic errors).

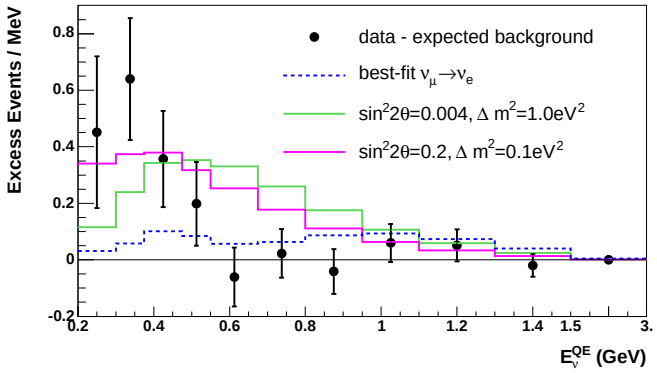

FIG. 2: The event excess as a function of E_ν^{QE}. Also shown are the expectations from the best oscillation fit and from neutrino oscillation parameters in the LSND allowed region [2]. The error bars include both statistical and systematic errors.

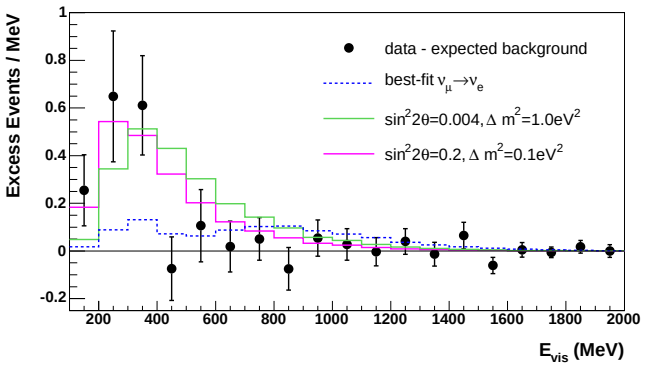

FIG. 3: The event excess as a function of E_{vis} for $E_\nu^{QE} > 200$ MeV. Also shown are the expectations from the best oscillation fit and from neutrino oscillation parameters in the LSND allowed region [2]. The error bars include both statistical and systematic errors.

TABLE III: *The χ^2 values from comparisons of the event excess Q^2 and $\cos(\theta)$ distributions for $300 < E_\nu^{QE} < 475$ MeV to the expected shapes from various NC and CC reactions. Also shown is the factor increase necessary for the estimated background for each process to explain the low-energy excess.*

Process	$\chi^2(cos\theta)$/9 DF	$\chi^2(Q^2)$/6 DF	Factor Increase
NC π^0	13.46	2.18	2.0
$\Delta \to N\gamma$	16.85	4.46	2.7
$\nu_e C \to e^- X$	14.58	8.72	2.4
$\bar{\nu}_e C \to e^+ X$	10.11	2.44	65.4

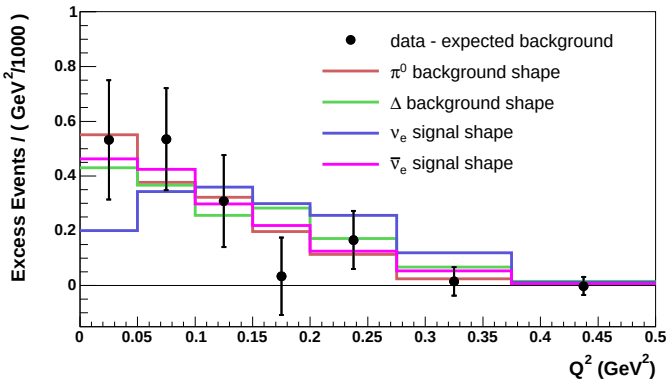

FIG. 4: The event excess as a function of Q^2 for $300 < E_\nu^{QE} < 475$ MeV. Also shown are the expected shapes from the NC π^0 and $\Delta \to N\gamma$ reactions, which are representative of photon events produced by NC scattering, and from CC $\nu_e C \to e^- X$ and $\bar{\nu}_e C \to e^+ X$ scattering. The error bars include both data statistical and shape-only systematic errors.

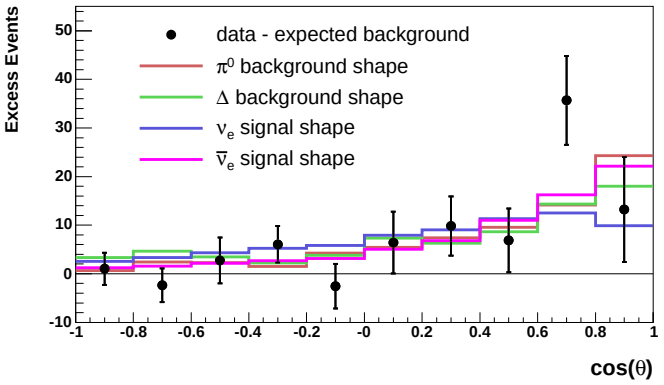

FIG. 5: The event excess as a function of $\cos(\theta)$ for $300 < E_\nu^{QE} < 475$ MeV. The legend is the same as Fig. 4.

like events in the energy region $200 < E_\nu^{QE} < 475$ MeV. These events are consistent with being either electron events produced by CC scattering ($\nu_e C \to e^- X$ or $\bar{\nu}_e C \to e^+ X$) or photon events produced by NC scattering ($\nu C \to \nu\gamma X$). Upcoming MiniBooNE results with the Booster antineutrino beam and with the NuMI neutrino beam [21] should help distinguish these two possibilities and shed further light on the low-energy region.

We acknowledge the support of Fermilab, the Department of Energy, and the National Science Foundation, and we acknowledge Los Alamos National Laboratory for LDRD funding. In addition, we acknowledge theoretical input from Tina Leitner and Ulrich Mosel on the $\Delta \to N\gamma$ background.

[1] A. Aguilar-Arevalo *et al.*, Phys. Rev. Lett. 98, 231801 (2007).

[2] C. Athanassopoulos *et al.*, Phys. Rev. Lett. 75, 2650 (1995); 77, 3082 (1996); 81, 1774 (1998); A. Aguilar *et al.*, Phys. Rev. D 64, 112007 (2001).

[3] As mentioned in reference [1], two analysis methods were used to analyze the data. The results of the two analyses agree, although the second method lacks sensitivity in the low-energy region. Therefore, the first analysis method is used in this paper. The second analysis is described in D.W. Schmitz, PhD Thesis, Columbia University (2008).

[4] Jeffrey A. Harvey, Christopher T. Hill, and Richard J. Hill, Phys. Rev. Lett. 99, 261601 (2007); Phys. Rev. D 77, 085017 (2008).

[5] Michel Sorel, Janet Conrad, and Michael Shaevitz, Phys. Rev. D 70, 073004 (2004); C. Karagiorgi *et al.*, Phys. Rev. D 75, 013011 (2007); Alessandro Melchiorri *et al.*, [arXiv:0810.5133].

[6] Heinrich Paes, Sandip Pakvasa, and Thomas J. Weiler, Phys. Rev. D 72, 095017 (2005).

[7] T. Goldman, G. J. Stephenson Jr., and B. H. J. McKellar, Phys. Rev. D 75, 091301 (2007).

[8] Michele Maltoni and Thomas Schwetz, Phys. Rev. D 76, 093005 (2007).

[9] Ann E. Nelson and Jonathan Walsh, Phys. Rev. D 77, 033001 (2008).

[10] V. Alan Kostelecky and Matthew Mewes, Phys. Rev. D 69, 016005 (2004); T. Katori, A. Kostelecky and R. Tayloe, Phys. Rev. D 74, 105009 (2006).

[11] A. Aguilar-Arevalo *et al.*, [arXiv:0806.4201], accepted by Nucl. Instrum. Meth. A.

[12] S. Agostinelli *et al.*, Nucl. Instrum. Meth. A506, 250 (2003).

[13] J. R. Sanford and C. L. Wang, Brookhaven National Laboratory, AGS internal reports 11299 and 11479 (1967) (unpublished) is used for pion production, and a Feynman scaling model is used for kaons.

[14] M. G. Catanesi *et al.* [HARP Collaboration], Eur. Phys. J. C52, 29 (2007).

[15] I. Chemakin *et al.*, Phys. Rev. C 77, 015209 (2008); T. Abbott *et al.*, Phys. Rev. D45, 3906 (1992); J. V. Allaby *et al.*, CERN 70-12 (1970); D. Dekkers *et al.*, Phys. Rev. 137, B962 (1965); G. J. Marmer *et al.*, Phys. Rev. 179, 1294 (1969); T. Eichten *et al.*, Nucl. Phys. B44, 333 (1972); A. Aleshin *et al.*, ITEP-77-80 (1977); I. A. Vorontsov *et al.*, ITEP-88-11 (1988).

[16] A. Aguilar-Arevalo *et al.*, [arXiv:0806.1449], submitted to Phys. Rev. D.

[17] D. Casper, Nucl. Phys. Proc. Suppl. 112, 161 (2002).

[18] A. A. Aguilar-Arevalo *et al.*, Phys. Lett. B. 664, 41 (2008).

[19] CERN Program Library Long Writeup W5013 (1993).

[20] C. Zeitnitz and T. A. Gabriel, Nucl. Instrum. Meth. A349, 106 (1994).

[21] P. Adamson *et al.*, [arXiv:0809.2447], submitted to Phys. Rev. Lett.